Bio-Design and Manufacturing (2024) 7:31–42
https://doi.org/10.1007/s42242-023-00257-z

RESEARCH ARTICLE

A novel integrated microfluidic chip for on-demand electrostatic droplet charging and sorting

Jinhui Yao[1] · Chunhua He[1] · Jianxin Wang[1] · Canfeng Yang[1] · Ye Jiang[1] · Zhiyong Liu[1] · Guanglan Liao[1] · Tielin Shi[1]

Received: 25 March 2023 / Accepted: 2 August 2023 / Published online: 25 November 2023

Abstract

On-demand droplet sorting is extensively applied for the efficient manipulation and genome-wide analysis of individual cells. However, state-of-the-art microfluidic chips for droplet sorting still suffer from low sorting speeds, sample loss, and labor-intensive preparation procedures. Here, we demonstrate the development of a novel microfluidic chip that integrates droplet generation, on-demand electrostatic droplet charging, and high-throughput sorting. The charging electrode is a copper wire buried above the nozzle of the microchannel, and the deflecting electrode is the phosphate buffered saline in the microchannel, which greatly simplifies the structure and fabrication process of the chip. Moreover, this chip is capable of high-frequency droplet generation and sorting, with a frequency of 11.757 kHz in the drop state. The chip completes the selective charging process via electrostatic induction during droplet generation. On-demand charged microdroplets can arbitrarily move to specific exit channels in a three-dimensional (3D)-deflected electric field, which can be controlled according to user requirements, and the flux of droplet deflection is thereby significantly enhanced. Furthermore, a lossless modification strategy is presented to improve the accuracy of droplet deflection or harvest rate from 97.49% to 99.38% by monitoring the frequency of droplet generation in real time and feeding it back to the charging signal. This chip has great potential for quantitative processing and analysis of single cells for elucidating cell-to-cell variations.

Graphic abstract

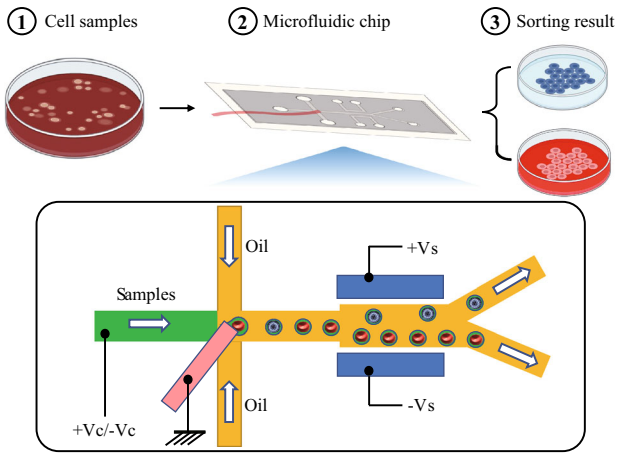

Keywords Copper wire · Droplet generation · Droplet sorting · Microfluidic chips · On-demand charging

Jinhui Yao and Chunhua He have contributed equally to this work.

✉ Zhiyong Liu
zhiyong_liu@hust.edu.cn

✉ Guanglan Liao
guanglan.liao@hust.edu.cn

Introduction

Droplet microfluidics is a novel and recently-developed technique for generating microdroplets [1, 2]. Encapsulating cells within droplets enables their use for single-cell analyses [3, 4], cell cultures [5, 6], in vitro organ models [7, 8], and disease modeling [9]. Microdroplets are generally manipulated by a variety of manipulation strategies including acoustic [10, 11], optical [12, 13], thermal [14], magnetic [15, 16], valve-based [17], hydrodynamic [18, 19], or electrical [20, 21]. Among them, the electrical method has unique advantage, including a short response time [22], easy setup, high integration [23], and good compatibility [24].

However, current methods for electrically sorting microdroplets necessitate the deposition of corresponding electrodes onto the substrate. Moreover, in some cases, they require specialized electrodes to contact the droplets, which complicates the fabrication process [25]. If droplets are deflected solely by dielectrophoretic force without prior charging, it is difficult to deflect individual droplets when they are moving at high speed. This is because deflecting electrodes are generally long, which results in all droplets within the region being deflected simultaneously [26]. Therefore, it is crucial to develop a novel microfluidic chip for the pre-charging of high-frequency droplets.

Guo et al. proposed a droplet sorting device that generated microdroplets using a flow focusing channel and deflected droplets directly using direct current (DC) voltage. This device was found to be able to separate individual mammalian cell-encapsulated alginate droplets. However, due to the lack of pre-charging, the droplet frequency was very low, reaching only 250 Hz; moreover, its sorting speed was quite slow [27]. Ahn et al. proposed a droplet-based microfluidic device for simultaneous droplet charging and sorting by electrostatic actuation. This device placed the sorting electrode immediately behind the location where droplets were generated. It induced electric charges on the surface of the droplet via the sorting electrode. The sorting electrode was then used to complete the sorting process, and realized an improved sorting throughput, but still, this reached a droplet frequency of 600 Hz only and necessitated the fabrication of a complex electrode structure [28]. In addition, Ahn et al. [29] proposed a droplet-based microfluidic device that integrated two separate modules: a hydrodynamic flow-focusing structure for generating water-in-oil droplets and two paired electrodes for charging and sorting these droplets. This device allowed robust control of individual droplets in the presence of positive, negative, or neutral charges. However, the device required the deposition of an indium tin oxide (ITO) electrode layer and an oxide insulating layer on the glass substrate, thereby complicating the preparation process. Rao et al. injected conductive silver paste into the polydimethylsiloxane (PDMS) cavity to make three-dimensional (3D) electrodes, replacing the traditional complex deposition and stripping process and simplifying the device fabrication. This device pre-charged droplets and then divided them into two halves for separate sorting, reaching a sorting efficiency of 95% [24, 30]. Vyawahare et al. designed a new microfluidic system for droplet sorting that reached a sorting purity exceeding 90%. However, this system required gold-plated electrodes and an insulating layer, and was still cumbersome to fabricate [31]. If droplets can be charged at the same time as they are generated, thus achieving high-throughput charged droplet generation, high-speed sorting of droplets can be easily achieved using a 3D-deflected electric field.

We therefore propose a novel integrated microfluidic chip for the on-demand generation and deflection of charged droplets. To construct this device, we buried a slender wire at the point of droplet generation. Charging of the droplets was achieved by induction of electricity from the copper wire, while deflection of the droplets was achieved through a 3D deflecting electrode within the microchannel. Since droplets are charged while they are generated, the droplets can be charged and sorted at a high throughput of 11 kHz, which is comparable to the sorting speed of flow cytometry [32, 33]. Importantly, our device is fully enclosed for droplet generation and sorting, and does not require a complex deposition and stripping process for electrode preparation. Moreover, we can arbitrarily control the number and ratio of deflected droplets. Finally, by feeding the realized monitored frequency of droplet generation back to the charging signal, the accuracy of droplet charging and deflection can reach 99.38%. This device may therefore be valuable in biomedical research for cell culturing and sorting.

Materials and methods

COMSOL simulation

To identify an optimal microchannel structure for droplet generation, we used COMSOL Multiphysics version 5.6 (COMSOL Inc., Cambridge, MA, USA) to simulate the effect of droplet generation under different nozzle widths. To simplify the simulation process, we adopted a two-dimensional model and made the following assumptions: (1) liquids behaved as Newtonian fluids, (2) no-slip boundary conditions were adopted, and (3) a compressible Stokes flow model was selected to represent the physics of our stationary model [34]. The boundary conditions in the simulation were set as shown in Table 1. Phosphate buffered saline (PBS) was used as the dispersed phase, and dimethyl silicone oil was

[1] State Key Laboratory of Intelligent Manufacturing Equipment and Technology, Huazhong University of Science and Technology, Wuhan 430074, China

Table 1 Boundary conditions for the nozzle structure simulation

Name	Boundary condition
Boundary	Viscosity, density, surface tension coefficient, and other parameters taken from the physical parameters of the two phases (i.e., water and oil) [35]
U_1	10 μL/min
U_2	80 μL/min
Outlet	Zero pressure
Other channel surfaces	Wall drainage and a contact angle of 135° [36]

U_1: flow rate of the dispersed phase; U_2: flow rate of the continuous phase

used as the continuous phase. We applied a boundary condition of +100 V at the entrance of the dispersed phase and set a grounded electrode in the nozzle to simulate the charging of droplets during generation. A stable parallel deflection electric field was then applied after the microdroplets were generated to realize droplet displacement.

Fabrication of the microfluidic chip

Fabrication of the microchannel template

First, a silicon wafer (Suzhou Research Material Micro-Nano Technology Corporation, China) was irradiated in an ultraviolet (UV)–ozone cleaner for 15 min to obtain a hydrophilic surface. SU8-2025 (MicroChem, USA) was then spin-coated onto the silicon wafer, which was then heated at 65 °C for 3 h (Figs. S1a and S1b in Supplementary Information). A mask with the microchannel pattern was then placed on the wafer, which was exposed to UV light for 15 s (Fig. S1c in Supplementary Information). The resulting silicon wafer was heated at 95 °C for 15 min, and then placed in propylene glycol methyl ether acetate developer (MicroChem, USA) and isopropyl alcohol (Sigma Aldrich, USA) for 15 s respectively for cyclic development until white precipitates no longer appeared [37]. Finally, the wafer was heated at 135 °C for 20 min, and its surface became hydrophobic due to the properties of $C_{16}H_{19}F_{17}O_3Si$ (MACKLIN, Shanghai, China) (Fig. S1d in Supplementary Information). This procedure concluded the preparation of the microchannel template.

PDMS inversion process

PDMS prepolymers and curing agent (SYLGARD 184 Silicone Elastomer Kit, Dow Corning, Midland, MI, USA) were mixed at a volume ratio of 10:1 to form mixed solution. The solution was first poured onto the microchannel template to form an insulation layer approximately 200 μm above the flow channel. We calculated the product of the surface area of the microchannel template and the total thickness of the insulation layer (approximately 250 μm) to obtain a value. The total volume of the microchannel was then subtracted from this value to determine the volume of solution required to create the PDMS insulation layer. After the PDMS had cured, we placed a slender copper wire with a diameter of approximately 150 μm at the nozzle where the droplets were generated. The charging electrode was produced in a relatively simple way. The remaining solution was poured onto the template to form a thicker PDMS microchannel (Fig. S1e in Supplementary Information). Finally, we cut and drilled the cured PDMS (Fig. S1f in Supplementary Information).

Chip packaging process

The PDMS microchannel and a glass substrate (CITOTEST, China) were bombarded in an oxygen plasma cleaner (Harrick Scientific, USA) to obtain activated surfaces (Figs. S1g and S1h in Supplementary Information). After the PDMS was treated with oxygen plasma, the -CH_3 groups in its surface layer disappeared and were replaced by -OH groups. After the glass was treated with oxygen plasma, its surface layer was filled with Si–OH bonds. The Si–OH bonds on the surface of PDMS and on the surface of glass formed stable and dense Si–O–Si bonds after dehydration reactions [38, 39]. We then bonded the two surfaces together and heated them at 95 °C for 7 h to complete the fabrication of the microfluidic chip (Fig. S1i in Supplementary Information).

Test system for the chip

Post-processing of the chip

Since the generation of water-in-oil droplets requires the microchannel to be hydrophobic [40], we subjected the prepared microfluidic chip to a hydrophobic treatment for 10 h using $C_{16}H_{19}F_{17}O_3Si$.

Microscopic characterization

The thickness of the PDMS insulation layer was measured under an optical microscope, as shown in Fig. S2 (Supplementary Information). The shape and size of the droplets were also observed by a high-speed camera (AcutEye-2 M-1000, Ketianjian Photoelectric Technology Corporation, China).

Materials and instruments required for testing

The dispersed phase (PBS buffer, 0.03 mol/L, pH=7.2, Codow, China) and continuous phase (dimethyl silicone

oil, PMX-200, SYLGARD, USA) were introduced into the chip by an injection pump (LSP02-3B, Baoding Dichuang Electronic Technology Corporation, China), polytetrafluoroethylene hoses, syringes, and microfluidic connectors. A laser generator (THORLABS, USA), a photodetector, and an oscilloscope (Tektronix TDS2012B, USA) were used to detect the frequency of droplet generation. A signal generator (Agilent 33250A, USA) and a voltage amplifier (Aigtek ATA-2161, Antai Electronic Technology Corporation, China) were used to generate pulsed signals to charge the microdroplets. Finally, positive and negative high-voltage direct current (DC) power supplies (DW-P303-1ACH2 and DW-N303-1ACH2, Dongwen High Voltage Power Supply Corporation, China) were used to generate the deflected electric field.

Results and discussion

Working mechanism

A structural diagram of the chip is shown in Fig. 1a. The positive or negative electrode of the charging structure is directly connected to the inlet of the dispersed phase, while the ground electrode is positioned above the microchannel nozzle with a thin PDMS layer interposed approximately 200 μm above the flow channel. The ground electrode, a slender copper wire, is then embedded in the chip during the PDMS curing process. This does not require lithography, coating, or other processes on the substrate, and only the embedding of the copper wire during PDMS curing is necessary. The four-layer structure of the chip is shown in Fig. 1b. Here, the copper wire is sandwiched between the PDMS insulation layer and the remaining PDMS. We then bond the side with the microchannel to a glass substrate to obtain the final microfluidic chip.

When no voltage is applied to the dispersed phase (Vc=0), droplets are generated according to the flow focusing structure. When a positive voltage is applied to the dispersed phase (Vc>0), positive charges are induced at the water–oil interface closest to the grounded copper wire near the nozzle due to electrostatic induction. After generation of the droplet, positive charges will remain on the surface of the droplet, thereby positively charging the droplet. The duration of electrostatic induction can be regulated by controlling the application time of the positive voltage to control the number of microdroplets per charging circle. Similarly, if a negative voltage is applied to the dispersed phase (Vc<0), negatively charged droplets will be generated. By precisely controlling the charging voltage, droplets can be generated and charged accurately on demand at the same time. As charged droplets pass through the droplet deflection area, the electrostatic force then causes positively charged droplets to move toward the negative pole and negatively charged ones toward the positive pole, thereby realizing on-demand deflection of droplets.

Our chips can be used for sorting cells or molecules after encapsulation in droplets. After being detected by other structures (e.g., by fluorescence detection, etc.), cells or molecules can be encapsulated in droplets and selectively charged at the same time. They are then deflected using an electric field based on their surface charge. Note that the sorting function of the chip is a priori, and does not involve changing the polarity of the sorting electrodes.

Fluid simulation

As shown in Fig. 2, the inlet widths of both the dispersed and continuous phases were uniformly set to 50 μm. The width of the outlet channel was set to 80 μm. The width of the nozzle used to generate the droplets was varied and denoted as W, as shown in Fig. 2a. The flow rates U_1 for the dispersed phase and U_2 for the continuous phase were set as shown in Table 1. Notably, W ranged from 30 to 70 μm (Fig. 2a-II–VI). In Fig. 2, red represents the dispersed phase and blue represents the continuous phase. When W=30 μm, both the dispersed and continuous phases flowed backward through the nozzle. Here, the pressure of the continuous phase exceeded that of the dispersed phase, impeding droplet formation at the nozzle and resulting in a post-nozzle jet type. The droplets generated in this case exhibited a larger diameter and a lower frequency of generation.

Moreover, when W increased to 40 μm, the squeezing pressure of the continuous phase relative to the dispersed phase decreased, and droplets were generated at the nozzle; however, the frequency of droplet generation was insufficient. When W=50 μm, the squeezing pressure of the continuous phase relative to the dispersed phase reached a suitable state. At this point, droplets were generated in the drop type at a high frequency, which can be seen from the spacing between droplets. The diameter of these droplets was approximately 37 μm, and they exhibited excellent monodispersity. When W was further increased to 60 and 70 μm, the squeezing pressure of the continuous phase relative to the dispersed phase weakened, resulting in a lower frequency of droplet generation. Therefore, based on these results, it can be concluded that the droplet generation state using this chip design was optimal when W=50 μm. Therefore, this nozzle structure was selected as the microstructure for microdroplet generation.

Under a bias of +100 V, a positively charged droplet shifted in the deflection electric field (as shown in Fig. 2b). During the first 20 μs, the droplet underwent weak deflection, but this effect was not yet obvious. However, at 60 μs, the droplet already underwent significant deflection. Since the droplet flowed to the right with the continuous phase, it

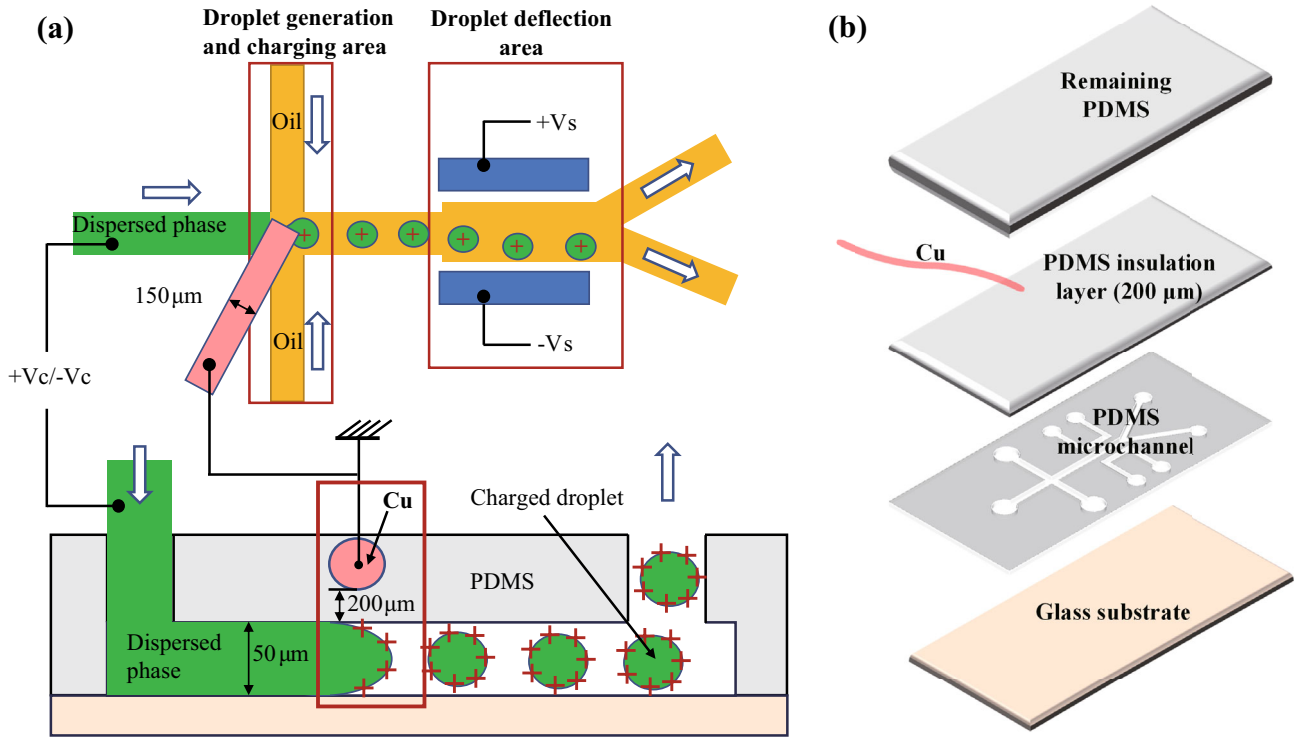

Fig. 1 Schematic diagram of the microfluidic chip: **a** the on-demand charging and deflection design, and **b** the four-layer structure of the chip. PDMS: polydimethylsiloxane

moved toward the right. At the same time, the droplet was charged. Thus, after we applied an upward horizontal electric field, the droplet was deflected upward as a way to simulate the deflection of a charged droplet in an electric field. After 100 μs, the droplet moved 25 μm horizontally and 12 μm vertically (Fig. 2b-VI). At this rate, the droplet would continue to deflect vertically until it separated from the other droplets.

The actual chip

An image of our integrated microfluidic chip is displayed in Fig. 3a. This shows a glass substrate, a PDMS microchannel, and a slender copper wire for on-demand charging and deflection of droplets. The PDMS microchannel consists of two functional regions: the droplet generation region (Fig. 3b) and the droplet deflection region (Fig. 3c). The inlet widths of the dispersed and continuous phases in the droplet generation structure are both 50 μm, and the width of the nozzle is also 50 μm, which is consistent with the COMSOL simulation results. The height of all flow channels is 50 μm. The deflection electrode used for the droplet deflection area adopts a 3D structure with the same height as the flow channel, which introduces PBS conductive solution during operation. The 3D electrode can therefore form a 3D electric field with sufficient electric field strength, eliminating the need for metal electrode plating on the glass and simplifying the chip fabrication process. The test system for the chip is shown in Fig. 3d.

Droplet formation and on-demand charging

We conducted an experimental investigation into the impact of the flow rate ratio between the continuous and dispersed phases on the droplet formation state to select the appropriate injection speed for the continuous phase. Thus, to explore the influence of flow rate on the frequency of droplet generation and the diameter of droplet, we analyzed the force state during droplet breakage and generation. When a droplet is generated at the nozzle, it is subjected to various forces, including the viscous force between two fluid phases, the inertial force of fluid flow in the dispersed phase, gravity, interfacial tension, and the shear force provided by the continuous phase. The inertial force and gravity are negligible because the Reynolds number of the fluid is very small on the microscopic scale. Interfacial tension, viscous force, and shear force are the main factors affecting the droplet generation process. The capillary number $C_a = \frac{\mu U_2}{\sigma}$ can be used to describe these three forces. Here, μ is the viscosity of the continuous phase, U_2 is the flow rate of the continuous phase, and σ is the interfacial tension between the two phases [41, 42].

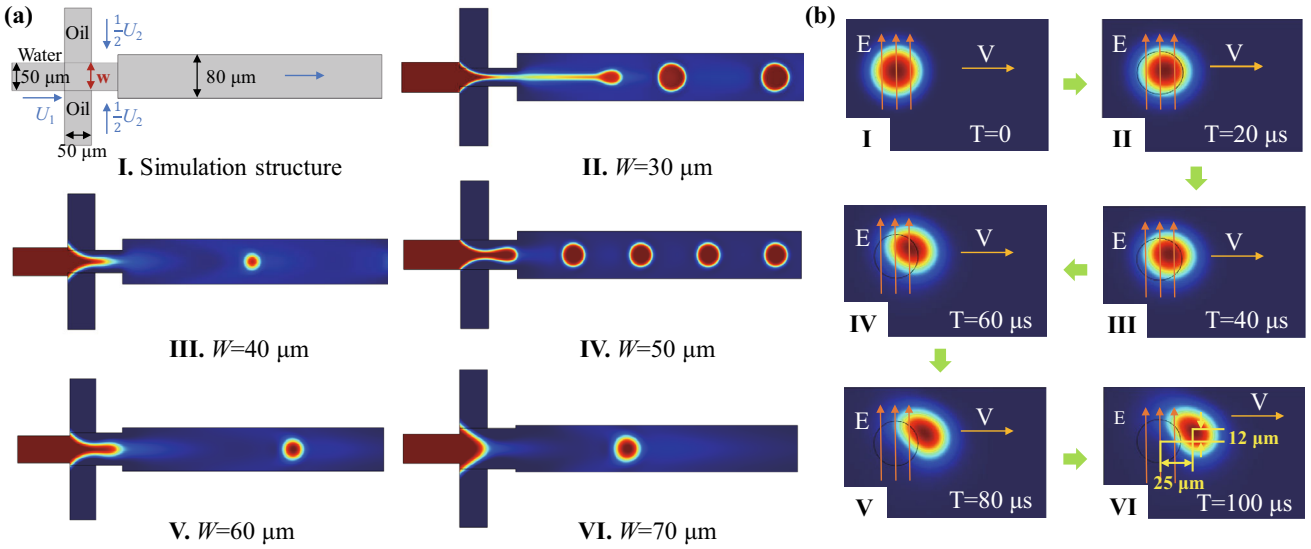

Fig. 2 **a** Two-dimensional numerical simulation of the nozzle structure for droplet generation. **b** Two-dimensional numerical simulation of the deflection of a charged droplet

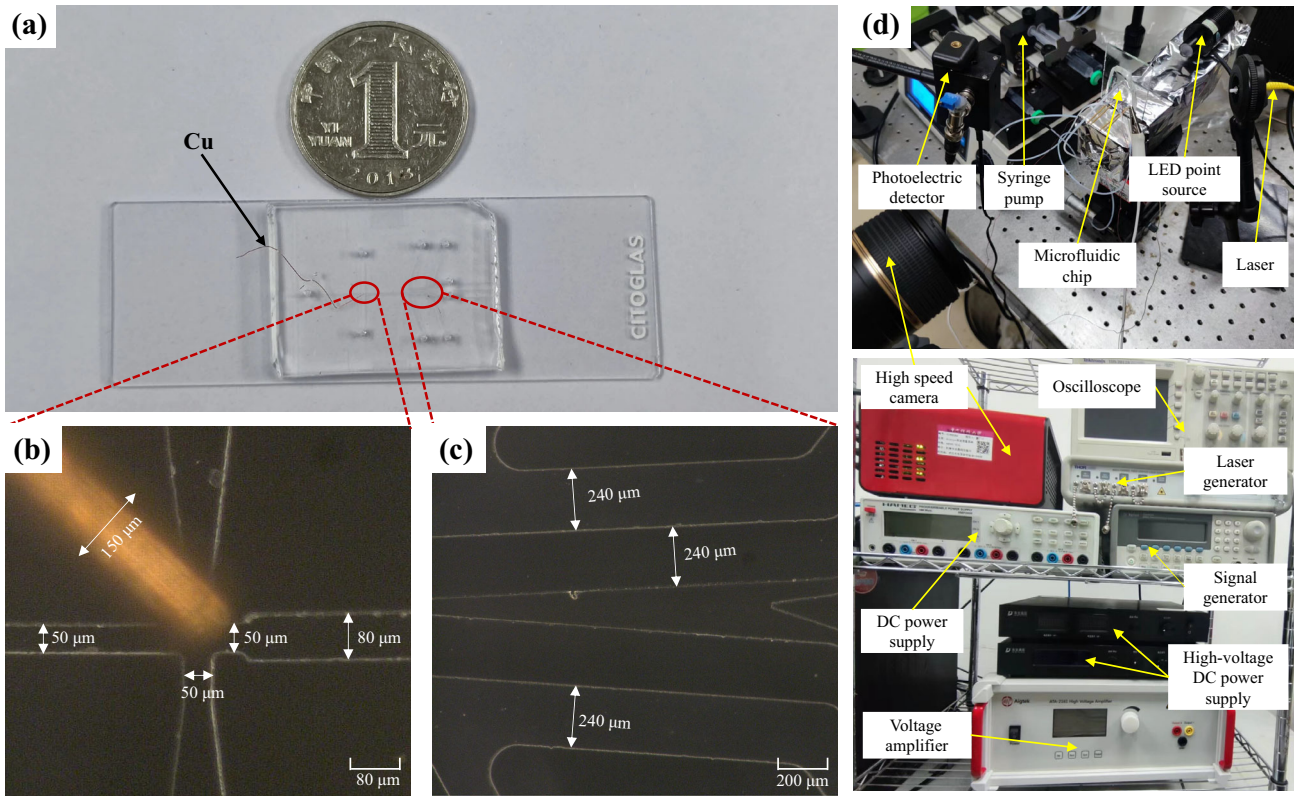

Fig. 3 **a** Authentic photograph of the chip. **b** Magnified view of the nozzle. **c** Magnified view of the droplet deflection region. **d** The test system for the chip. LED: light emitting diode; DC: direct current

The formation of droplets is attributed to the shear force provided by the continuous phase, which overcomes the interfacial tension between the two phases. The shear force provided by the continuous phase is proportional to the flow rate of the continuous phase. Therefore, when the viscosity of the continuous phase and the surface tension of the two phases are both fixed, a higher flow rate of the continuous phase facilitates easier droplet formation [43]. Hence, we

investigated the effect of the continuous phase flow rate on droplet generation frequency and droplet size.

To facilitate clear observation of the droplet generation process, the copper wire was positioned beside the nozzle without applying a charging voltage. A microstructure was then used to passively generate droplets. During experimentation, we kept the flow rate of the dispersed phase at 10 μL/min, adjusted the injection pump to change the flow rate of the continuous phase, and observed and measured the frequency of droplet generation and the diameter of the droplet. We experimented with the nozzle width set to 50 μm and the flow rate of the dispersed phase set at 10 μL/min (Fig. 4a). When the flow rate of the continuous phase was between 30 and 50 μL/min, the capillary number was low, and the droplet generation state was the squeeze type. In this state, the frequency of droplet generation was low, the diameter of the droplet was larger than the width of the nozzle, and the monodispersity of droplets was good (Fig. 4b and Video S1 in Supplementary Information). However, when the flow rate of the continuous phase was 50–110 μL/min, the capillary number increased, and the droplet generation state was the drop type. In this state, the frequency of droplet generation was high, the diameter of the droplet was small (i.e., smaller than the width of the nozzle), and the droplet was monodispersed (Fig. 4c). When the flow rate of the continuous phase was 90 μL/min, the frequency of droplet generation was 11.757 kHz, and the diameter of individual droplets was approximately 33 μm. The diagram of the gradual increase in the volume of the droplet at the nozzle until it broke during one cycle is shown in the Supplementary Information (Fig. S3). In addition, when the flow rate of the continuous phase exceeded 110 μL/min, the capillary number became too large, resulting in the jet type droplet generation state. In this state, the frequency of droplet generation was lower than that when the flow rate of the continuous phase was 110 μL/min. The droplet diameter was smaller than the width of the nozzle, and the droplets were polydisperse (Fig. 4d and Video S3 in Supplementary Information). Furthermore, when the flow rate of the continuous phase was 110 μL/min, droplet formation occurred at a critical state between the drop and jet types.

To study whether charging voltage has a significant impact on passive droplet generation, we buried the copper wire at the nozzle and applied a charging voltage. The experiment was conducted with a dispersed phase flow rate of 10 μL/min and a continuous phase flow rate of 90 μL/min. After droplets were stably generated, we recorded the frequency and diameter of droplet generation (Figs. 4a and 4c). For this experiment, we applied charging voltages of +20, +40, +60, +80, +100, +120, +140 V, etc., to the droplets, and then observed and recorded the state of droplet generation. When the charging voltage was below 260 V, the frequency and diameter of droplets generated during charging were comparable to those generated without charging (Fig. 4e). The distance between adjacent droplets was 76 μm. These droplets were generated and moved at a uniform speed, which means that droplet charging had no effect on droplet generation under these conditions. It ensured the stability of droplet generation when a rectangular wave or pulsed voltage was applied to the droplets to achieve on-demand droplet charging.

However, when the charging voltage reached or exceeded 280 V, we observed significant changes in the state of droplet formation. At this point the droplets were no longer generated and moved at a constant speed. The distance between adjacent droplets became uneven at intervals of 90, 96, and 78 μm, etc., as shown in Fig. 4f. This was because there were excessive charges on the droplets, making the droplets repel each other. Moreover, during droplet formation, those droplets with surplus charges were affected by electric field forces. Excessive electrophoretic forces resulted in inhomogeneous droplet formation, thereby disrupting the original equilibrium state and leading to a disordered state that is no longer conducive to on-demand charging of droplets.

In addition, our oil-in-water droplet generation strategy has been demonstrated to have no impact on cellular activity [44]. The oil used here was dimethyl silicone oil, whose main component is PDMS. PDMS is biocompatible and does not cause toxicity or damage to biological samples or cells [45]. On the other hand, the proposed droplet sorting strategy based on charging and deflecting also has a negligible impact on the activity of cells since they are encapsulated within oil phase droplets, and the charges are distributed on the droplet surface [46].

On-demand high-speed deflection of charged droplets under an electric field

To verify that droplets were indeed charged after the charging process, the deflection area was positioned downstream of the area where the microdroplets were generated. Within the deflection area, the upper side of the flow channel was connected to the negative electrode and the lower side was connected to the positive electrode. Uncharged droplets were electrically neutral and were therefore unaffected by the force of the electric field. The uncharged droplets would flow out of the lower channel due to the restriction of the outlet channel structure. In contrast, the positively and negatively charged droplets would move toward the negative and positive electrodes, respectively, under the action of the electric field force F_E. Therefore, positively charged droplets would flow out of the upper channel, while negatively charged droplets would flow out of the lower channel (Fig. 5a).

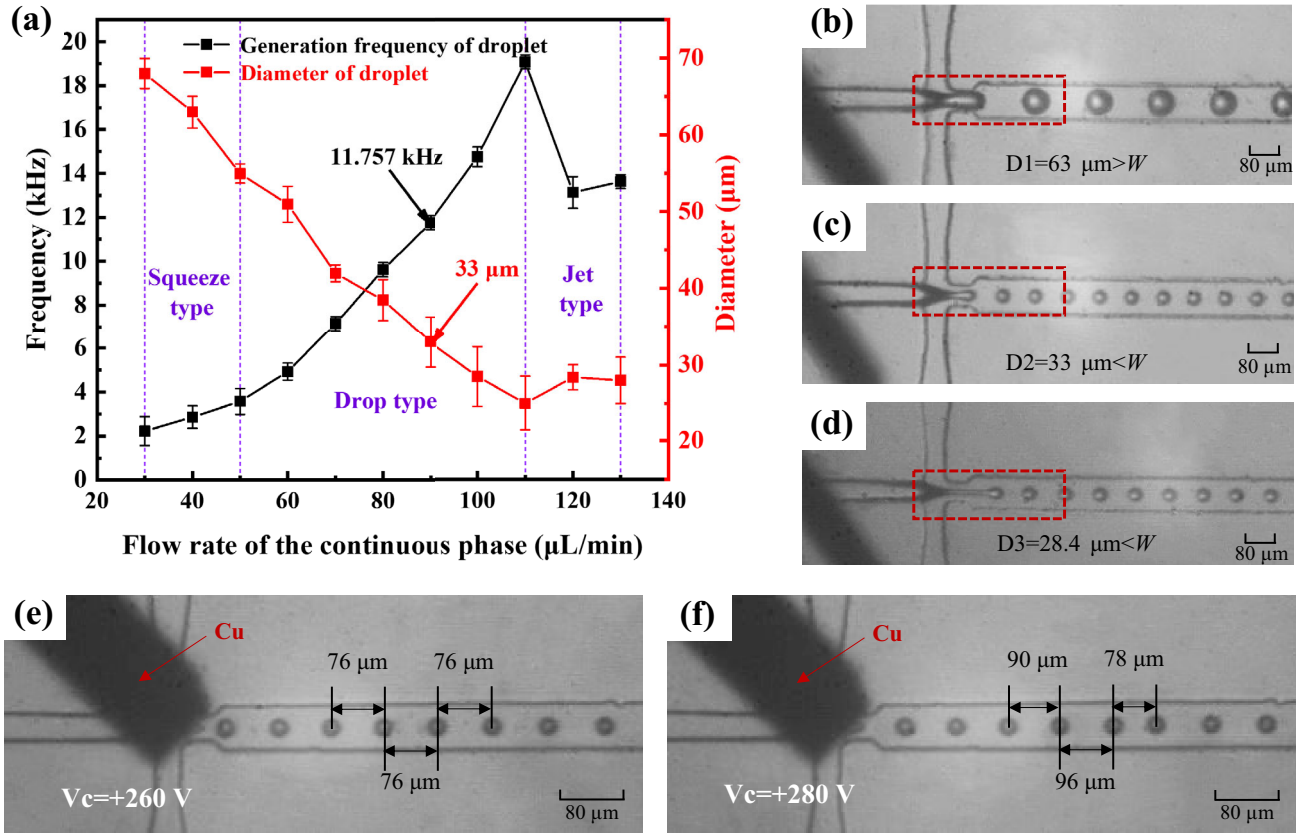

Fig. 4 **a** Variation curve of the frequency and diameter of droplet generation with changing flow rate of the continuous phase (data are represented as mean±standard deviation, n=5) . **b** Squeeze state of droplet formation when the flow rate of the continuous phase was 40 μL/min (Video S1 in Supplementary Information). **c** Drop state of droplet formation when the flow rate of the continuous phase was 90 μL/min (Video S2 in Supplementary Information). **d** Jet state of droplet formation when the flow rate of the continuous phase was 120 μL/min (Video S3 in Supplementary Information). **e** When the charging voltage was 260 V, it had no obvious effect on the droplet formation state. **f** When the charging voltage was 280 V, the droplet generation state was affected; droplet generation became uneven, and the droplets were not equidistantly spaced

In this experiment, we injected samples at a flow rate of 10 μL/min for the dispersed phase and 90 μL/min for the continuous phase. Figure 5b shows that droplets were directed to the lower channel due to the microstructure when the charging and deflection voltages were not applied. At this moment, the frequency of droplet generation was 11.757 kHz, and the period of droplet generation was approximately 85 μs.

A rectangular wave signal (Vc) was then applied to charge the droplets. The charging period was twice the droplet generation period. During each cycle, half of the period applied +100 V while the other half applied −100 V (Fig. 5c). In this way, droplets were generated successively according to the rule that one droplet was positively charged and the other droplet was negatively charged alternately. When the charged droplets flowed to the deflection area, one droplet moved toward the negative pole while the other moved toward the positive pole: this movement alternated, as shown in Fig. 5c. Furthermore, another rectangular wave signal with a period three times that of droplet generation was applied to the droplets. This signal consisted of +100 V for one-third of the period and −100 V for two-thirds of the period. In this way, the droplets would be generated successively according to the rule that one droplet was positively charged and two droplets were negatively charged, alternately. Thus, when the charged droplets flowed to the deflection area, they exhibited an alternating phenomenon of one droplet moving toward the negative pole and two moving toward the positive pole, as shown in Fig. 5d.

Similarly, by manipulating the charging voltage, a phenomenon of one droplet moving toward the negative pole and three moving toward the positive pole was also realized, as shown in Fig. 5e. The phenomenon that four droplets moved toward the negative pole and one moved toward the positive pole was also realized, as shown in Fig. 5f. Since our chip charges droplets as they are generated, the droplets can be successfully deflected on demand in the deflection region, no

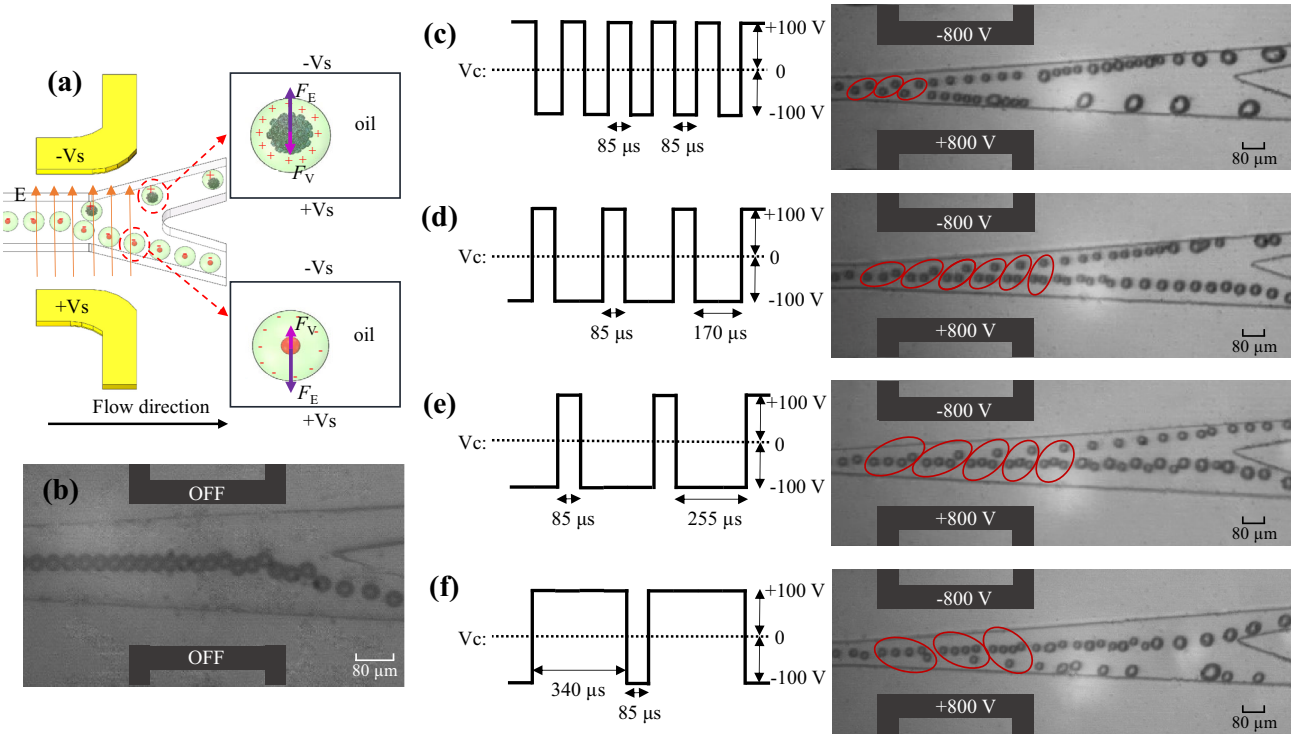

Fig. 5 **a** Schematic diagram of the deflection area. **b** Without deflection and charging voltage, all droplets flowed out from the lower channel under the microstructure. **c** One droplet moved toward the negative pole and the other moved toward the positive pole (Video S4 in Supplementary Information). **d** One droplet moved toward the negative pole and two moved toward the positive pole (Video S5 in Supplementary Information). **e** One droplet moved toward the negative pole and three moved toward the positive pole (Video S6 in Supplementary Information). **f** Four droplets moved toward the negative pole and one moved toward the positive pole (Video S7 in Supplementary Information)

matter how high the droplet frequency is, as long as they can be charged smoothly.

A new strategy for droplet charging

Since we used a passive droplet generation structure, instability of channel pressure, possibly due to minor errors in syringe pump feeding, or the deformation of PDMS could cause variation in the frequency of droplet generation. Moreover, if we charged the droplet according to a measured fixed frequency of droplet generation, the accuracy of droplet deflection would also fluctuate within a small range due to small fluctuations in droplet frequency. In this regard, we used a laser generator and a photodetector to detect the frequency of droplet passage within the flow channel, used an oscilloscope to pick up this frequency value and sent it to a computer. The computer then transmitted the frequency value to a signal generator, which charged droplets based on the real-time frequency value (Fig. 6a). More specifically, we tested three sets of experiments to observe the instability of the droplet generation frequency. The frequency of droplet generation was recorded every five minutes for each set of experiments, which was 12 times in total. The frequency of droplet generation fluctuated between 11.56 and 11.96 kHz, with an average value of approximately 11.757 kHz (Fig. 6b). As shown in Fig. 6c, our real-time charging method effectively enhanced the accuracy of droplet deflection from 97.49% to 99.38%. Our system requires prior knowledge of the droplets to be sorted and selectively charges them based on previous detection results. The deflecting electrode of the chip only provides a stable electric field and does not act as a selective role.

Table 2 summarizes the main technical parameters of our chip as well as previous chips used for droplet sorting. These results show that our chip exhibits superior performance in terms of droplet flux and deflection accuracy. Moreover, its fabrication process is simple and low-cost, and it provides a practical solution for microfluidic chip-based droplet sorting.

Conclusions

In this work, we proposed a novel integrated microfluidic chip for on-demand electrostatic droplet charging and sorting. The charging of droplets was achieved by burying a copper wire in the PDMS microchannel, while the deflection

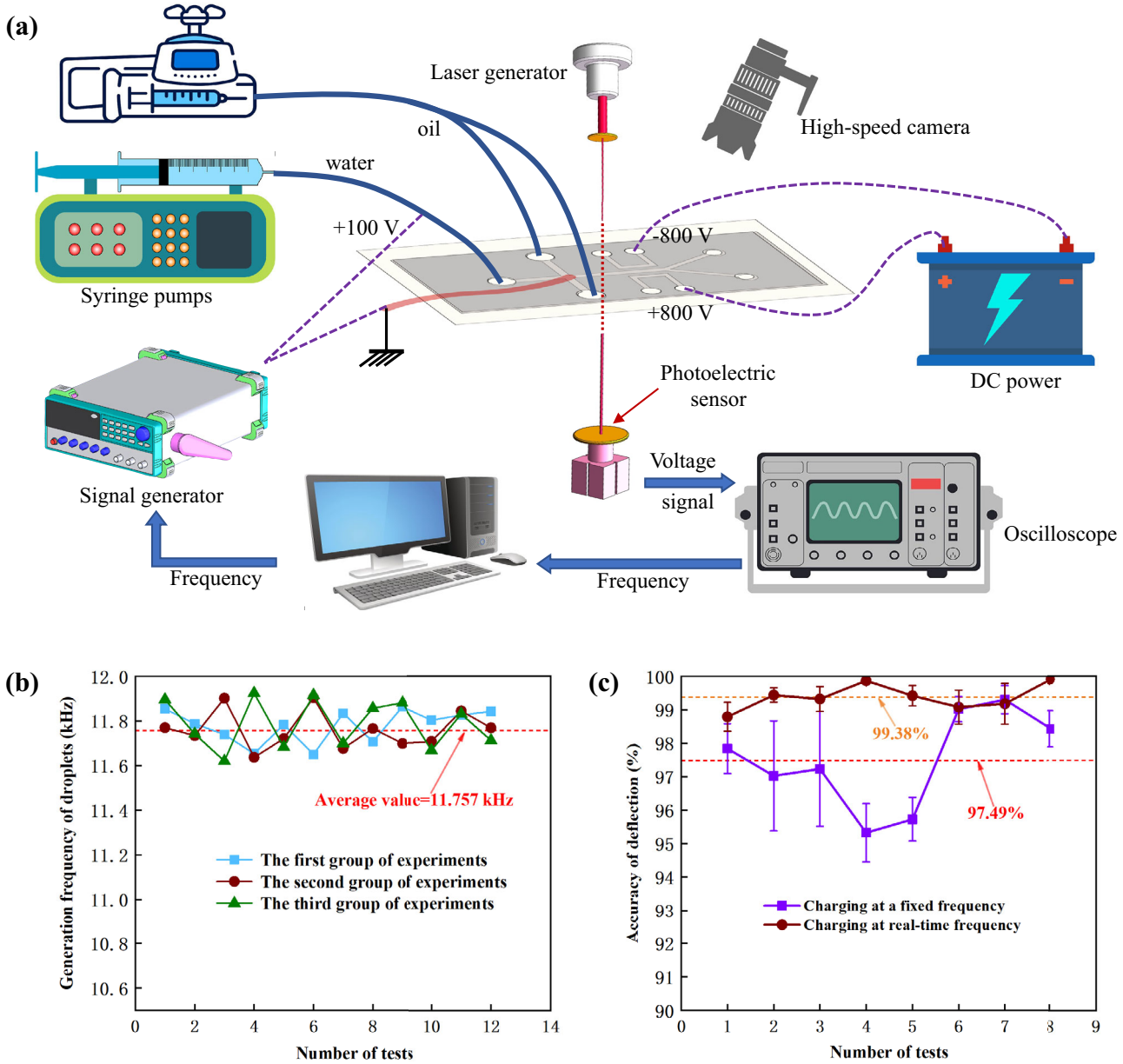

Fig. 6 **a** Schematic of the chip test system. Here, we monitored the frequency of droplet generation in real time and fed this frequency value to a signal generator to guide the on-demand charging of droplets. **b** Instability of the frequency of droplet generation at injection speeds of 10 and 90 μL/min for dispersed and continuous phases, respectively. **c** Accuracy of droplet deflection when charging droplets at a fixed frequency and at the real-time frequency of droplet generation (data are represented as mean±standard deviation, *n*=5)

Table 2 Comparison of the technical parameters between this chip and the previous chips used for droplet sorting

Device structure	Sorting speed	Sorting accuracy	Process complexity	Reference
This work	10 μL/min, 11.757 kHz	99.38%	Simple	–
Guo et al.	250 Hz	–	Complex	[27]
Ahn et al.	600 Hz	–	Complex	[28]
Ahn et al.	90 μL/h	–	Complex	[29]
Rao et al.	5 Hz	95%	Simple	[30]
Vyawahare et al.	4 kHz	>90%	Complex	[31]

of charged droplets was implemented by injecting PBS into the PDMS microcavity. The chip used a flow-focused passive structure to generate microdroplets and charged them via electrostatic induction during the droplet generation process. Importantly, the preparation process of this chip for droplet charging and deflection is relatively simple. Experimental results demonstrated that the chip achieved credible droplet generation, charging, and deflection at a high frequency of 11.757 kHz. The chip can control the number and ratio of deflected droplets arbitrarily according to our requirements. Furthermore, the accuracy of droplet charging and deflection increased from 97.49% to 99.38% by monitoring the frequency of droplet generation in real time and feeding it back to the charging signal. Our work provides a practical platform for on-demand droplet sorting, and shows considerable promise for biomedical applications such as cell sorting and single-cell analysis.

Supplementary Information The online version contains supplementary material available at https://doi.org/10.1007/s42242-023-00257-z.

Acknowledgements The authors acknowledge the financial support from the National Natural Science Foundation of China (No. 52275562) and the Technology Innovation Fund of Huazhong University of Science and Technology (No. 2022JYCXJJ015). The authors would like to express gratitude to the Analytical and Testing Center, Flexible Electronics Research Center, Measurement Laboratory of Collaborative Innovation Center, and the Wuhan National Laboratory for Optoelectronics of Huazhong University of Science and Technology for their assistance with lithography, coating, bonding, and characterization.

Author contributions JHY and CHH designed the experiments. JHY fabricated the microfluidic chip and integrated the chip with experimental observations and the detection device. JHY performed the simulation of the microstructure used for droplet generation and optimized the structural parameters of the microfluidic channel with the help of CHH. With the help of CHH and JXW, JHY conducted the experimental tests of droplet generation and deflection and summarized the laws and influencing factors of droplet generation and deflection. Together with CFY, JHY built a real-time droplet frequency detection system to improve the accuracy of droplet deflection. JHY compiled experimental data and wrote this manuscript together with CHH and YJ. GLL, TLS, and ZYL carefully guided the experimental tests and the writing of the manuscript. All authors reviewed the final version of the manuscript prior to submission.

Declarations

Conflict of interest The authors declare that they have no conflict of interest.

Ethical approval This article does not contain any studies with human or animal subjects performed by any of the authors.

References

1. Joensson HN, Andersson Svahn H (2012) Droplet microfluidics—a tool for single-cell analysis. Angewandte Chemie Int Ed 51(49):12176–12192. https://doi.org/10.1002/anie.201200460
2. Mashaghi S, Abbaspourrad A, Weitz DA et al (2016) Droplet microfluidics: a tool for biology, chemistry and nanotechnology. Trends Analyt Chem 82:118–125. https://doi.org/10.1016/j.trac.2016.05.019
3. Fan WH, Chen X, Ge YQ et al (2019) Single-cell impedance analysis of osteogenic differentiation by droplet-based microfluidics. Biosens Bioelectron 145:111730. https://doi.org/10.1016/j.bios.2019.111730
4. Matuła K, Rivello F, Huck WT (2020) Single-cell analysis using droplet microfluidics. Adv Biosyst 4(1):1900188. https://doi.org/10.1002/adbi.201900188
5. Terrell JA, Jones CG, Kabandana GKM et al (2020) From cells-on-a-chip to organs-on-a-chip: scaffolding materials for 3D cell culture in microfluidics. J Mater Chem B 8(31):6667–6685. https://doi.org/10.1039/d0tb00718h
6. Shih SCC, Barbulovic-Nad I, Yang XN et al (2013) Digital microfluidics with impedance sensing for integrated cell culture and analysis. Biosens Bioelectron 42:314–320. https://doi.org/10.1016/j.bios.2012.10.035
7. Bein A, Shin W, Jalili-Firoozinezhad S et al (2018) Microfluidic organ-on-a-chip models of human intestine. Cell Mol Gastroenterol Hepatol 5(4):659–668. https://doi.org/10.1016/j.jcmgh.2017.12.010
8. Tanataweethum N, Trang A, Lee C et al (2022) Investigation of insulin resistance through a multiorgan microfluidic organ-on-chip. Biomed Mater 17(2):025002. https://doi.org/10.1088/1748-605X/ac4611
9. Jalili-Firoozinezhad S, Miranda CC, Cabral JM (2021) Modeling the human body on microfluidic chips. Trends Biotechnol 39(8):838–852. https://doi.org/10.1016/j.tibtech.2021.01.004
10. Qin XM, Wei XY, Li L et al (2021) Acoustic valves in microfluidic channels for droplet manipulation. Lab Chip 21(16):3165–3173. https://doi.org/10.1109/MEMS51782.2021.9375309
11. Li PX, Ma ZC, Zhou YN et al (2019) Detachable acoustophoretic system for fluorescence-activated sorting at the single-droplet level. Anal Chem 91(15):9970–9977. https://doi.org/10.1021/acs.analchem.9b01708
12. Jiao L, Chen R, Ye DD et al (2019) Optical droplets sorting assisted by superhydrophobic surface with hydrophilic patterns. Int J Heat Mass Transf 143:118560. https://doi.org/10.1016/j.ijheatmasstransfer.2019.118560
13. Blaha ME, Hasan S, Dusny C et al (2022) Fluorescence lifetime activated droplet sorting (FLADS) for label-free sorting of *Synechocystis* sp. PCC6803. Lab Chip 22(8):1604–1614. https://doi.org/10.1039/D2LC00032F
14. Khater A, Abdelrehim O, Mohammadi M et al (2021) Thermal droplet microfluidics: from biology to cooling technology. Trends Analyt Chem 138:116234. https://doi.org/10.1016/j.trac.2021.116234
15. Zheng CX, Zhou S, Chen X et al (2021) Effect of oersted field on the localized droplet mode and propagating spin waves mode excited in spin-torque nano-oscillator. J Magn Magn Mater 539:168379. https://doi.org/10.1016/j.jmmm.2021.168379
16. Buryk-Iggers S, Kieda J, Tsai SSH (2019) Diamagnetic droplet microfluidics applied to single-cell sorting. AIP Adv 9(7):075106. https://doi.org/10.1063/1.5095884
17. Unger MA, Chou HP, Thorsen T et al (2000) Monolithic microfabricated valves and pumps by multilayer soft lithography. Science 288(5463):113–116. https://doi.org/10.1126/science.288.5463.113
18. Yoon DH, Numakunai S, Nakahara A et al (2014) Hydrodynamic on-rail droplet pass filter for fully passive sorting of droplet-phase samples. RSC Adv 4(71):37721–37725. https://doi.org/10.1039/c4ra08354g

19. Yoon K, Jung HW, Chun MS (2020) Two-phase flow in microfluidic-chip design of hydrodynamic filtration for cell particle sorting. Electrophoresis 41(10–11):1002–1010. https://doi.org/10.1002/elps.201900394
20. Sun HZ, Ren YK, Hou LK et al (2019) Continuous particle trapping, switching, and sorting utilizing a combination of dielectrophoresis and alternating current electrothermal flow. Anal Chem 91(9):5729–5738. https://doi.org/10.1021/acs.analchem.8b05861
21. Schütz SS, Beneyton T, Baret JC et al (2019) Rational design of a high-throughput droplet sorter. Lab Chip 19(13):2220–2232. https://doi.org/10.1039/c9lc00149b
22. Ahmadi F, Samlali K, Vo PQ et al (2019) An integrated droplet-digital microfluidic system for on-demand droplet creation, mixing, incubation, and sorting. Lab Chip 19(3):524–535. https://doi.org/10.1039/c8lc01170b
23. Clark IC, Thakur R, Abate AR (2018) Concentric electrodes improve microfluidic droplet sorting. Lab Chip 18(5):710–713. https://doi.org/10.1039/c7lc01242j
24. Rao L, Cai B, Wang JL et al (2015) A microfluidic electrostatic separator based on pre-charged droplets. Sens Actuat B Chem 210:328–335. https://doi.org/10.1016/j.snb.2014.12.057
25. Zhang YY, Zheng TT, Wang L et al (2021) From passive to active sorting in microfluidics: a review. Rev Adv Mater Sci 60(1):313–324. https://doi.org/10.1515/rams-2020-0044
26. Xi HD, Zheng H, Guo W et al (2017) Active droplet sorting in microfluidics: a review. Lab Chip 17(5):751–771. https://doi.org/10.1039/c6lc01435f
27. Guo F, Ji XH, Liu K et al (2010) Droplet electric separator microfluidic device for cell sorting. Appl Phys Lett 96(19):193701. https://doi.org/10.1063/1.3360812
28. Ahn B, Lee K, Louge R et al (2009) Concurrent droplet charging and sorting by electrostatic actuation. Biomicrofluidics 3(4):044102. https://doi.org/10.1063/1.3250303
29. Ahn B, Lee K, Panchapakesan R et al (2011) On-demand electrostatic droplet charging and sorting. Biomicrofluidics 5(2):024113. https://doi.org/10.1063/1.3604393
30. Rao L, Cai B, Yu XL et al (2015) One-step fabrication of 3D silver paste electrodes into microfluidic devices for enhanced droplet-based cell sorting. AIP Adv 5(5):057134. https://doi.org/10.1063/1.4921317
31. Vyawahare S, Brundage M, Kijac A et al (2021) Sorting droplets into many outlets. Lab Chip 21(21):4262–4273. https://doi.org/10.1039/d1lc00493j
32. Lim SW, Abate AR (2013) Ultrahigh-throughput sorting of microfluidic drops with flow cytometry. Lab Chip 13(23):4563–4572. https://doi.org/10.1039/c3lc50736j
33. Vazquez JM, Parrilla I, Roca J et al (2009) Sex-sorting sperm by flow cytometry in pigs: issues and perspectives. Theriogenology 71(1):80–88. https://doi.org/10.1016/j.theriogenology.2008.09.044
34. Grimmer A, Hamidović M, Haselmayr W et al (2019) Advanced simulation of droplet microfluidics. ACM J Emerg Technol Comput Syst 15(3):26. https://doi.org/10.1145/3313867
35. Lashkaripour A, Abouei Mehrizi A, Rasouli M et al (2015) Numerical study of droplet generation process in a microfluidic flow focusing. J Comput Appl Mech 46(2):167–175. https://doi.org/10.22059/JCAMECH.2015.55101
36. Yang G, Chu X, Vaikuntanathan V et al (2020) Droplet mobilization at the walls of a microfluidic channel. Phys Fluid 32(1):012004. https://doi.org/10.1063/1.5139308
37. Elvira KS, Gielen F, Tsai SS et al (2022) Materials and methods for droplet microfluidic device fabrication. Lab Chip 22(5):859–875. https://doi.org/10.1039/d1lc00836f
38. Xiong LC, Chen P, Zhou QS (2014) Adhesion promotion between PDMS and glass by oxygen plasma pre-treatment. J Adhes Sci Technol 28(11):1046–1054. https://doi.org/10.1080/01694243.2014.883774
39. Borók A, Laboda K, Bonyár A (2021) PDMS bonding technologies for microfluidic applications: a review. Biosensors 11(8):292. https://doi.org/10.3390/bios11080292
40. Li LH, Yan ZB, Jin ML et al (2019) In-channel responsive surface wettability for reversible and multiform emulsion droplet preparation and applications. ACS Appl Mater Interfaces 11(18):16934–16943. https://doi.org/10.1021/acsami.9b03160
41. Han WB, Chen XY, Wu ZL et al (2019) Three-dimensional numerical simulation of droplet formation in a microfluidic flow-focusing device. J Braz Soc Mech Sci Eng 41(6):265. https://doi.org/10.1007/s40430-019-1767-y
42. Yousofvand R, Ghasemi K (2022) A novel microfluidic device for double emulsion formation: the effects of design parameters on droplet production performance. Colloids Surf A Physicochem Eng Aspects 635:128059. https://doi.org/10.1016/j.colsurfa.2021.128059
43. Lei L, Zhao Y, Chen W et al (2021) Experimental studies of droplet formation process and length for liquid–liquid two-phase flows in a microchannel. Energies 14(5):1341. https://doi.org/10.3390/en14051341
44. Schaerli Y, Hollfelder F (2009) The potential of microfluidic water-in-oil droplets in experimental biology. Mol Biosyst 5(12):1392–1404. https://doi.org/10.1039/B907578J
45. Raj MK, Chakraborty S (2020) PDMS microfluidics: a mini review. J Appl Polymer Sci 137(27):48958. https://doi.org/10.1002/app.48958
46. Sun G, Teng Y, Zhao Z et al (2020) Functional stem cell sorting via integrative droplet synchronization. Anal Chem 92(11):7915–7923. https://doi.org/10.1021/acs.analchem.0c01312